Effects of Cumulus Entrainment and Multiple Cloud Types on a January Global Climate Model Simulation

MAO-SUNG YAO

Centel Federal Services Corporation, Institute for Space Studies, New York, New York

ANTHONY D. DEL GENIO

NASA/Goddard Space Flight Center, Institute for Space Studies, New York, New York

(Manuscript received 12 December 1988, in final form 10 February 1988)

ABSTRACT

An improved version of the GISS Model II cumulus parameterization designed for long-term climate integrations is used to study the effects of entrainment and multiple cloud types on the January climate simulation. Instead of prescribing convective mass as a fixed fraction of the cloud base grid-box mass, it is calculated based on the closure assumption that the cumulus convection restores the atmosphere to a neutral moist convective state at cloud base. This change alone significantly improves the distribution of precipitation, convective mass exchanges and frequencies in the January climate. The vertical structure of the tropical atmosphere exhibits quasi-equilibrium behavior when this closure is used, even though there is no explicit constraint applied above cloud base. Global aspects of the simulation using the neutral buoyancy closure are almost identical to those obtained in a previous study with a closure relating cumulus mass flux explicitly to large-scale forcing.

A prescription of 0.2 km^{-1} for the fractional rate of entrainment lowers the peak of the convective heating profile, reduces equatorial specific humidities in the upper atmosphere to more realistic values, and greatly increases eddy kinetic energy at the equator due to reduced momentum mixing. With two cloud types per convective event, each cloud type having a prescribed size and entrainment rate, a clear bimodal distribution of convective mass flux is obtained in strong convective events. At the same time, many of the desirable climate features produced by the neutral buoyancy and entrainment experiments are preserved.

1. Introduction

Even though the spatial and temporal scales of cumulus clouds are much smaller than that of large-scale atmospheric motions, their effect on the latter is of utmost importance in the heating of the tropical atmosphere (Riehl and Malkus 1958). The goal of a cumulus parameterization is to represent the collective effects of both deep and shallow cumuli on large-scale motions without explicitly simulating each cumulus cloud. Simulations of the atmospheric general circulation and climate have a significant dependence on the cumulus parameterization (Baker et al. 1977; Yao and Stone 1987; Del Genio and Yao 1988). Cloud feedbacks and the response of surface temperature to changes in forcing in a climate model may also depend on the cumulus parameterization (Lindzen et al. 1982; Del Genio and Yao 1988). Therefore, an adequate and computationally efficient cumulus parameterization is very desirable for climate simulation and climate sensitivity studies.

Corresponding author address: Dr. Anthony D. Del Genio, NASA/GSFC, Institute for Space Studies, 2880 Broadway, New York, NY 10025.

The most widely used cumulus parameterizations in global climate models (GCMs) can generally be classified into three categories: 1) moist adiabatic adjustment (Manabe et al. 1965), 2) the Kuo (1965, 1974) scheme, and 3) the Arakawa and Schubert (1974) scheme. Moist adiabatic adjustment has the appeal of simplicity, but it is difficult to relate the adjustment process to actual physical processes which modify the atmosphere on the large scale. This scheme forces the lapse rate in the tropics to be close to moist adiabatic (Wetherald and Manabe 1988), which is less steep than observed (Betts 1986). Kuo's scheme has a clearer physical picture of warming of the environment by cumulus clouds, although the mechanism it invokes is not generally accepted (Yanai 1971). Arakawa and Schubert's scheme is by far the most sophisticated cumulus parameterization proposed to date. It solves for convective mass fluxes, entrainment rates and a cloud spectrum simultaneously by assuming the existence of a quasi-equilibrium between a cumulus ensemble and the large-scale forcing. However, this method is relatively difficult to implement (Lord et al. 1982) and may require too much computing time for routine use in very long-term climate simulations.

The cumulus parameterization developed at GISS

(Hansen et al. 1983) for the Model II GCM is easy to apply and computationally efficient. It is based on the theory of warming and drying the environment by compensating downward motion and is similar in some respects to early versions of the Arakawa scheme. However, as noted by Del Genio and Yao (1988; hereafter referred to as DY88), it uses the mass of an arbitrarily chosen fraction (50%) of the cloud-base grid box for the cumulus convective mass and is likely to overestimate the magnitude of convective transports and cloud feedback. In DY88, the GISS Model II cumulus parameterization is used, but the cumulus mass fluxes are calculated explicitly by a formula which may include the large-scale forcings of low-level convergence, surface evaporation and the effect of varying boundary layer height. An alternative approach is to estimate the mass fluxes required to relax the atmosphere to a quasi-neutral state in response to such forcings. The quasi-equilibrium concept implies that these two different approaches should give similar results when averages over a suitably long time are taken. In this paper we test this assertion by calculating the cumulus fluxes implicitly in a way that is qualitatively similar to Arakawa and Schubert's (1974) quasi-equilibrium assumption but is simplified for application to long-term climate problems.

Arakawa and Schubert (1974) postulated a full spectrum of cumulus clouds with different cloud top levels in part because a parameterization with only a single cloud type is likely to produce an excessively dry lower troposphere in regions of deep cumulus convection. Yanai et al. (1973) also stressed the importance of the coexistence of shallow clouds with deep clouds in maintaining the large-scale heat and moisture budgets. In Arakawa and Schubert's scheme the variable which defines the cloud spectrum is the fractional rate of entrainment. (In actual computations the model levels define the cloud spectrum, and the parameterization determines the fractional entrainment rate needed for the cloud to reach that level.) Lord (1982) has performed semiprognostic tests with observed large-scale forcing to illustrate the role of entrainment in the Arakawa–Schubert scheme. However, the effects of entrainment and a cloud spectrum on a fully interactive global climate model simulation are difficult to predict. In this paper, we add entrainment and a crude cumulus spectrum (i.e., multiple cloud types) to the moist convection scheme in the GISS global climate model, and investigate their effects on a January climate simulation.

In section 2, we review in detail the basic thermodynamics of the GISS cumulus parameterization with given cumulus mass fluxes. In section 3, we describe the closure assumption that we use to determine implicitly the cumulus fluxes. The inclusion of entrainment and a crude cumulus spectrum is presented in section 4. We discuss results obtained with the GISS global climate model in section 5. A summary and conclusions are given in section 6.

2. Basic cumulus parameterization

The cumulus parameterization in the most recent version of the GISS GCM (Hansen et al. 1983, hereafter referred to as Model II) creates a single plume (or cloud type) which rises out of the cloud base layer whenever it is moist-convectively unstable with respect to the layer above and is not diluted by entrainment; the environment is warmed and dried by the induced subsidence. Condensation, precipitation and reevaporation of cloud droplets occur as the saturated plume rises and the condensate falls through the unsaturated environment. In Hansen et al. (1983), the description of this parameterization is quite brief. Here we give a more detailed account of the computational algorithm and numerical schemes to provide a context for the discussion of a new closure assumption, entrainment and multiple cloud types in the following sections.

The plume mass, M_c, is arbitrarily chosen as half the air mass, M_a, of the cloud base grid-box in Model II. For now it suffices to assume that once

$$h_l = c_p\theta_l + Lq_l > h^*_{l+1} = c_p\theta_{l+1} + Lq^*_{l+1}, \quad (1)$$

a convective plume of mass M_c (per physics time step) forms at the cloud-base level $l = LB$ (see Fig. 1), where l is the index for the vertical levels, θ the potential temperature, q the specific humidity, c_p the specific heat at constant pressure, L the latent heat of evaporation,

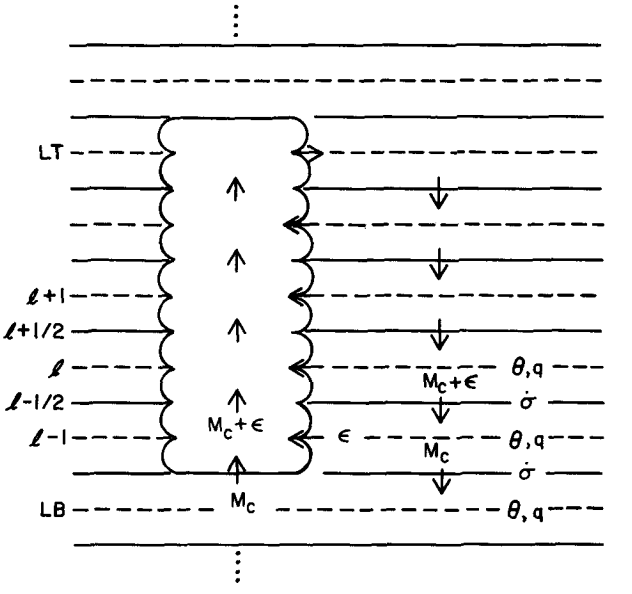

FIG. 1. Schematic diagram of the cumulus model and the staggered grid for vertical differencing. Solid and dashed lines represent layer edges and interiors, respectively; $\dot{\sigma}$ is the vertical velocity in σ-coordinates; other symbols are defined in text.

and h the moist static energy. ($s = c_p\theta$ is an approximate form of the dry static energy per unit mass.) Condition (1) is the criterion for moist convective instability at cloud base. The instability test (1) is performed first at the lowest model level ($l = 1$) and then at higher levels up to the tropopause until the first unstable layer is found. In practice, most convection (77%) originates from $l = 1$.

The plume, as it leaves its base, carries with it the dry static energy $M_c s_{LB}$ and water vapor $M_c q_{LB}$. As the plume rises and is saturated, it condenses an amount of water vapor, C. Thus its dry static energy becomes $(M_c s_{LB} + LC)$ and its water vapor decreases to $(M_c q_{LB} - C)$. The condensate C remains in the layer in which it forms and may become part of the precipitation. The plume, maintaining its mass, can go higher as long as its moist static energy (which is conserved as it rises in undilute ascent) is larger than the environment's saturated moist static energy. The plume reaches its top level, LT, when this condition is no longer met; at $l = LT$ the plume detrains and mixes with the environment. At the same time, the environment at levels $LB \leq l < LT$ is warmed and dried by the induced subsidence of environmental air from the layer above and is adjusted as follows:

$$M_a s_l \rightarrow M_a s_l + M_c c_p(\theta_{l+1} - \theta_l), \quad (2)$$

$$M_a q_l \rightarrow M_a q_l + M_c(q_{l+1} - q_l). \quad (3)$$

The same equations apply to the mixing of plume and environment at the detrainment level LT if $l + 1$ and l are replaced by LB and LT, respectively.

The convective cloud cover, f_c, is determined as M_c/M_a (somewhat different from the formula given in Hansen et al. 1983). The liquid water condensed from the plume, starting from LT, drops to the next lower layer and reevaporates to the extent that it saturates $f_c/2$ of the environment at that level. The remaining condensate drops to the next level, combines with the condensate produced at that level, and the process is repeated. Below cloud base, falling condensate is allowed to saturate a fraction f_c of the environment instead. The vertically integrated liquid water remaining after the consideration of reevaporation accounts for the convective precipitation.

The same computational cycle will take place if after the convection the atmosphere is still convectively unstable at any level above the cloud base. Thus, in principle the algorithm can produce an instantaneous spectrum of clouds, with one LT for each LB. However, experience shows that multiple convective events at a given grid box and time step are infrequent.

Cumulus friction, which is needed for attaining the desired Hadley circulation strength in Model II (Hansen et al. 1983), is also included, and is treated in a way similar to the dry static energy. This process is a major sink of tropospheric kinetic energy, since the model contains no explicit diffusion.

3. The closure assumption and computation of M_c

Generally speaking, a closure assumption is needed in a cumulus parameterization for determination of the cumulus mass (or mass flux). In Model II, M_c is arbitrarily chosen as half the grid box air mass of the cloud base layer. Even though the Model II GCM simulates the general features of the climate reasonably well (Hansen et al. 1983), it gives an unsatisfactory representation of several aspects of the tropical circulation and hydrologic cycle (DY88). A more sensible closure assumption is required to increase confidence in the predictions of GCM climate sensitivity experiments.

To address the closure problems, Arakawa and Schubert (1974) introduced an integral measure of the buoyancy force in convective clouds called the "cloud work function," $A(\lambda)$. Here, λ is taken to be the fractional rate of entrainment, and is used to define a spectrum of clouds of different heights; $A(\lambda) > 0$ is a generalized criterion for moist convective instability. It includes contributions from the buoyancy at cloud base, the integrated conditional instability above cloud base, and the reduction of buoyancy due to entrainment of environmental air. Their well known "quasi-equilibrium assumption" is $dA(\lambda)/dt \approx 0$. As originally envisioned by Arakawa and Schubert, the quasi-equilibrium states were quasi-neutral to convection [$A(\lambda) \approx 0$]. In application of the quasi-equilibrium assumption in GCMs, however, the atmosphere is adjusted to empirically determined, nonzero values of $A(\lambda)$ for the tropics and subtropics after higher values of $A(\lambda)$ are produced by the large-scale forcing associated with other GCM processes (Lord et al. 1982). The values of λ required to give each cloud type vanishing buoyancy at the discrete GCM vertical levels are solved for iteratively at each time step.

For the purpose of long-term climate simulations, we seek a similar approach to closure, but we are limited by two constraints. First, we require a simple, computationally efficient parameterization which permits decadal-scale integrations to be run routinely. In addition, we desire a scheme which exhibits quasi-equilibrium behavior but does not relax the atmosphere automatically to a particular value of the cloud work function. This is not an issue for simulations of the current climate, because $A(\lambda)$ does not vary greatly from one region to another (Lord and Arakawa 1980). However, in a changing climate, such as that due to increasing trace gas amounts, lapse rate and humidity changes may correlate in such a way as to produce slight changes in $A(\lambda)$, and these will have a nonnegligible feedback on surface temperature (Hansen et al. 1984). Since it is not yet possible to predict $A(\lambda)$ from first principles, we cannot assume that its current values apply universally to other climatic states with different radiative forcing. The ideal parameterization for cli-

mate change experiments is therefore one which predicts a quasi-equilibrium state without specifying it as an input. Such a closure would permit $A(\lambda)$ to remain either constant or vary slowly as the climate changes.

The closure assumption that we will use here is, to a certain extent, similar to that of Arakawa and Schubert (1974) and to an earlier parameterization by Arakawa (1972). We solve for the M_c that will make $h_{LB} = h^*_{LB+1}$ after the moist convection event has occurred, i.e., the cumulus mass flux that restores the cloud base to neutral buoyancy relative to the next higher layer. The atmosphere structure above cloud base is then determined by the effects of subsidence and detrainment as given by (2) and (3), and by the reevaporation of falling condensate. In particular, the atmosphere may still be conditionally unstable after the convection, i.e., $dh^*/dz < 0$, but the humidity at LB has been reduced to an extent which prevents further convection from being triggered. This results in a more realistic vertical structure than that produced by moist convective adjustment. Furthermore, since we do not adjust automatically to an observed value of the cloud work function, the scheme has the flexibility to produce any combination of lapse rate and humidity changes [and thus different $A(\lambda)$] in response to changes in climate forcing.

We need to use an iteration method to reach the condition $h_{LB} = h^*_{LB+1}$. In principle, we can compute the convective plume mass which exactly restores the atmosphere to the neutral state by repeating the convective cycle described in section 2, using the iteration method of halving the interval (Gerald 1980), starting with a first guess of $M_c/M_a = 0.5$ (the value used in Model II). This technique converges to an accuracy of 0.2% within ≤ 9 iterations. However, it is not computationally economical to do this. The layers above $LB + 2$ influence the stability at cloud base only through the evaporation of falling condensate. In the experiments discussed in section 5, we obtain an approximate solution for M_c by using the liquid water condensed in the layer $LB + 1$ as a rough estimate of the condensate available for reevaporation at $LB + 1$; the effect of precipitation generated above $LB + 1$ is neglected. The solution obtained will be exact if the reevaporation of precipitation is not considered, and if the plume indeed rises above $LB + 1$; if the plume detrains at $LB + 1$, the solution will be slightly in error.

Our experience indicates that the solution for M_c obtained by the approximated method is computationally economical and is usually within 20% of the exact solution. The M_c obtained this way is typically a few percent of M_a, consistent with available estimates and far more accurate than the arbitrarily prescribed fraction used in Model II (see the discussion in section 5). Furthermore, the computational accuracy can be increased at will if the computer time is not a consideration.

4. Entrainment and multiple cloud types

In the cumulus parameterization used in Model II, plumes rise undiluted by colder, drier environmental air. While this may accurately represent the behavior of protected updraft cores in deep convective towers, it is not characteristic of cumulus clouds in general. Entrainment of surrounding air reduces the buoyancy of updrafts and limits the altitude to which they can penetrate. An ensemble of clouds with different entrainment rates will therefore exhibit a spectrum of cloud top heights. The effect is thus a change in the vertical profile of cumulus mass flux, resulting in a redistribution of heat, moisture and momentum.

Unfortunately, a reliable physical basis for calculating entrainment rates does not currently exist. Several different mechanisms for entrainment seem to be present within cumulus clouds. Lateral entrainment associated with mesoscale pressure gradients in cloud clusters often gives rise to precipitation downdrafts (Knupp and Cotton 1985); we have attempted to crudely model this process in previous experiments (DY88). Here our concern is the smaller scale, cloud-top entrainment associated with turbulence at the cloud–environment interface (Paluch 1979). Little is known about this process other than the fact that low entrainment is usually associated with deep high clouds, and vice versa. Simpson et al. (1965) proposed a fractional entrainment rate inversely proportional to cloud radius based on similarity considerations and plume theory. However, the validity of this assumption is not necessarily borne out by observations (Sloss 1967).

In GCM applications of Arakawa and Schubert (1974), e.g., Lord et al. (1982), the fractional rate of entrainment, $\lambda = (1/M_c)(dM_c/dz)$ (where z is height), is the value for which the plume loses buoyancy at a given GCM level. Our goal is to examine the sensitivity of the GCM climate simulation to the presence of entrainment. Therefore, we simply choose a representative value for λ within the observed range and let the model determine the level the plume can reach with the given λ. While entrainment turns out to be important for obtaining realistic humidity and kinetic energy in the upper atmosphere, our results are not overly sensitive to the precise value of λ (see section 5).

When entrainment exists, the convective plume increases its mass as follows:

$$(M_c)_{l+1/2} = (M_c)_{l-1/2}(1 + \lambda\Delta z) = (M_c)_{l-1/2} + \epsilon_l, \quad (4)$$

where

$$\Delta z = z_{l+1/2} - z_{l-1/2}.$$

Equation (4) is subject to the further condition that $(M_c)_{l+1/2} \leq (M_a)_l$.

Due to the entrainment, the plume's properties are modified as follows:

$$(M_c s_c)_{l+1/2} \rightarrow (M_c s_c)_{l-1/2} + (\epsilon s_a)_l, \quad (5)$$

$$(M_c q_c)_{l+1/2} \rightarrow (M_c q_c)_{l-1/2} + (\epsilon q_a)_l, \quad (6)$$

where the subscript c refers to the plume and the subscript a refers to the environment. The environment loses dry static energy and moisture $(\epsilon s_a)_l$ and $(\epsilon q_a)_l$, respectively.

In Arakawa and Schubert (1974), λ is used to represent a cumulus spectrum with as many potential cloud types at any instant as there are model levels above the boundary layer. We may crudely represent a cumulus spectrum by breaking the single plume into two or more pieces, each with a prescribed fractional rate of entrainment. Thus, $M_c = M_1 + M_2 + \cdots M_I$, where I is the number of plumes. Correspondingly λ_1, $\lambda_2, \ldots \lambda_I$ (in increasing value of λ) are associated with $M_1, M_2, \ldots M_I$. The basic computational cycle discussed in section 2 is performed first for M_1 with λ_1. Then the computational cycle is repeated for M_2 with λ_2, and so on. Thus, the plume rising first has a suppressing effect on the plume rising later; but this effect turns out to be very small in the cases we have examined. Computation time increases linearly with I. Since active tropical convective systems usually display a bimodal distribution of convective fluxes (Johnson 1976; Nitta 1978), a reasonable assumption for climate model purposes is to set $I = 2$ with λ_1 and λ_2 characteristic of deep and shallow cumulus, respectively. The actual cloud top heights at any time step will, of course, vary with the degree of conditional instability of the atmosphere. Our prescription therefore produces a complete spectrum of cloud types when integrated over several time steps while preserving the tendency for deep and shallow convection to occur simultaneously over large areas. Our approach is supported by analyses of ISCCP data for the tropical Atlantic and Africa which show that instantaneous cumulus ensembles within GCM grid box-sized regions usually contain only one or two deep convective cloud types (Del Genio and Yao 1987).

The remaining problem is how to partition M_c between the two cloud types. In the Arakawa–Schubert scheme the spectrum is determined by the specified final state. No such constraint exists in the framework of the cumulus parameterization described here. In section 5, we test the sensitivity of the January climate simulation to the spectral distribution by systematically varying M_1 and M_2 from 0 to M_c. The approach of prescribing the number of cloud types and their sizes has also been used by Albrecht (1983).

5. Experiments with GISS global climate model II

To test the sensitivity of the current climate to the parameterization of cumulus clouds, we have conducted several experiments (see Table 1) in perpetual January mode with the GISS global climate model II (Hansen et al. 1983). The model was run at 8° × 10° horizontal resolution with nine vertical levels and with fixed climatological sea surface temperatures. Each experiment was run for four months; the diagnostics shown here represent averages over the last three months. For a full description of the model and its climatology, see Hansen et al. (1983).

TABLE 1. Details of experiments discussed in this paper. All except the control run use the neutral buoyancy closure assumption.

Experiment	Description
Control	GISS Model II (1 plume, $\lambda = 0$ km^{-1})
A	1 plume, $\lambda = 0$ km^{-1}
B	1 plume, $\lambda = 0.2$ km^{-1}
C	$M_1 = 0.5M_c$, $\lambda_1 = 0$ km^{-1}
	$M_2 = 0.5M_c$, $\lambda_2 = 0.2$ km^{-1}
D	$M_1 = 0.25M_c$, $\lambda_1 = 0$ km^{-1}
	$M_2 = 0.75M_c$, $\lambda_2 = 0.2$ km^{-1}

The control experiment in Table 1 is the same as that described in DY88. It specifies the convective mass to be one-half the mass of the cloud base grid box per physics time step whenever (1) is satisfied. Aside from some minor differences described in that paper, the control is effectively the standard version of Model II used in Hansen et al. DY88 present figures, for the control experiment, of cumulus mass exchange, relative humidity, total cloud cover, deep convection frequency (defined as all events that penetrate at least 4 GCM levels) and shallow convection frequency (defined as all events that penetrate no farther than GCM level 3).

Despite the simplicity of Model II's cumulus mass flux prescription, the control produces a reasonable simulation of most aspects of the January (and July as well) climate compared to other GCMs. However, some deficiencies exist, as noted by DY88: 1) A tendency to produce peak precipitation at 12°N due to excessive convection in the Bay of Bengal, Indochina, and over the warm waters west of Central America; 2) too much water vapor in the upper troposphere and too little in the lower troposphere in the tropics compared to observations; 3) a deficit of longwave eddy kinetic energy in the tropics; 4) deep convection occurrence frequencies of 10–15% in the most strongly convective regions of the ITCZ, well below the 50%–80% frequency estimated for 8° × 10° areas in the ISCCP Pilot Data Set by Del Genio and Yao (1987).

In each of the other experiments (A–D), the convective mass per physics time step, M_c, is calculated based on the closure assumption discussed in section 3. Experiments A–D differ from each other in their entrainment rates, the number of plumes per convective event, and the mass weighting of the plumes. Many details of the climate simulations are similar in these runs; we focus here only on significant changes between experiments.

Experiment A, which differs from the control only in its calculation of M_c, demonstrates the soundness of the neutral buoyancy closure assumption. The mass exchange per convective event in this experiment is about 7%–10% of the mass of the cloud base grid box (3.7–5 mb h^{-1}), which is close to observations (Johnson 1980) and much less than the arbitrary 50% specified in Model II. Deep convection frequencies, which are generally <10% in the control (see Fig. 2 of DY88) because of its large mass flux per event, are greatly increased relative to the control as a result (Fig. 2), to a more desirable 70%–90% in strong convective regions (Del Genio and Yao 1987). Shallow convection frequencies also increase, especially off the west coasts of North America, South America, Africa, and Australia (Fig. 3). The changes in occurrence frequency and mass flux per event do not exactly compensate: the time-averaged cumulus mass exchange is greatly reduced, particularly in the lower atmosphere (Fig. 4). Globally, the reduction in cumulus mass exchange is 26%. Since our closure assumption represents an upper limit on the possible M_c, the implication is that Model II overstabilizes the atmosphere. This is evident in the moist static energy profiles produced by the two experiments. At 4°N latitude $\Delta h = h(959\text{ mb}) - h(634\text{ mb}) = 7.3\text{ J g}^{-1}$ in the control but 9.4 J g^{-1} in Experiment A. A similarly defined Δh^* increases from 6.0 to 8.6 J g^{-1}. Thus, although our closure scheme neutralizes the cloud base relative to the next higher layer after each event, it preserves a substantial degree of conditional instability in the atmosphere above cloud base, i.e., $A(\lambda) > 0$, as is observed in the tropics. This contrasts with the behavior of moist convective adjustment, which effectively sets $A(\lambda) = 0$.

The reduced convection associated with the new closure scheme has a significant positive impact on the tropical general circulation and hydrologic cycle. For example, the peak precipitation, cumulus mass flux, and vertical velocity all shift from 12°N to 4°N. The reduction in precipitation is especially noticeable in the Bay of Bengal and Indochina, where the Model II simulation is quite poor (Fig. 5). Despite this, the strength of the Hadley cell remains relatively unchanged; this insensitivity was also apparent in our previous experiments (DY88).

A stringent test of our closure assumption is its ability to reproduce a quasi-equilibrium structure for the current climate, since this is not specified a priori. Arakawa and Chen (1987) have noted that for the deepest clouds ($\lambda = 0$), negative correlations between fluctuations in

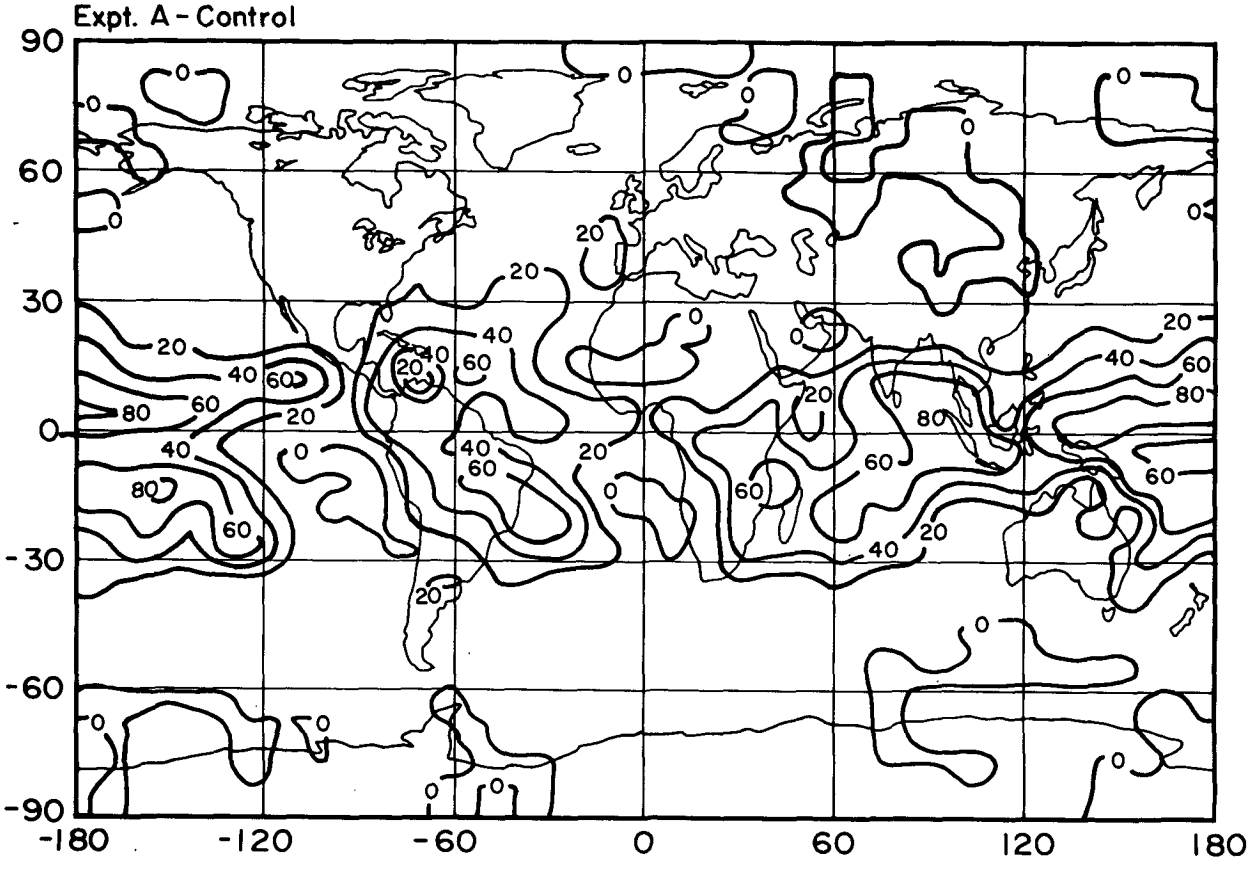

FIG. 2. Geographical distribution of differences in deep convection occurrence frequency (%) between Expt. A and the control.

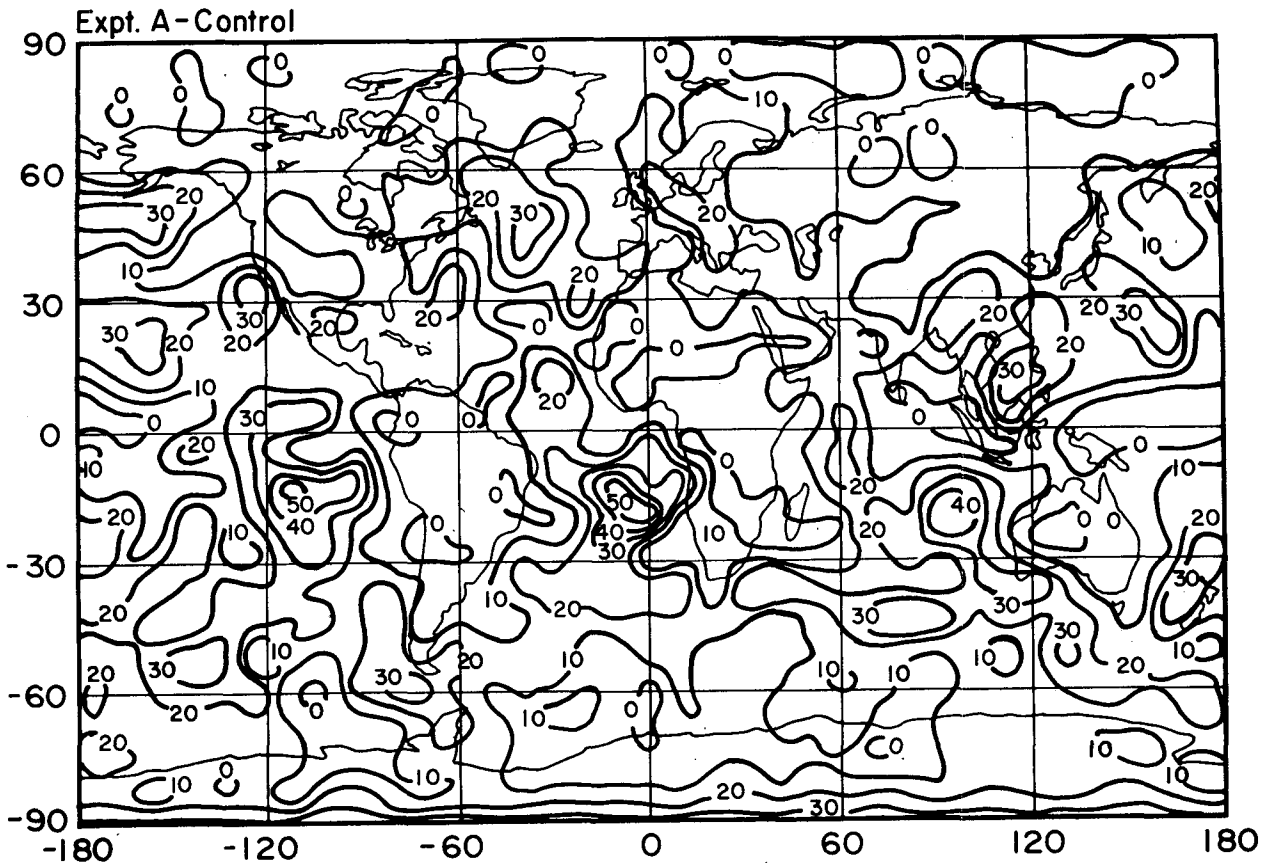

FIG. 3. As in Fig. 2 but for differences in shallow convection occurrence frequency (%).

relative humidity at cloud base and conditional instability above cloud base characterize a quasi-equilibrium state. In moist static energy terms this implies that ($h_{LB} - h^*_{LB}$) should increase as $-dh^*/dz$ decreases, and vice versa. Figure 6 compares the evolution of these two quantities over the last 24 hours of the control and Experiment A simulations at tropical land and ocean gridpoints. In both locations, the variations of relative humidity and lapse rate are largely uncorrelated in the control run, because the cumulus mass flux is independent of large-scale conditions. The final state is far removed from the initial state. Both of these indicate that large variations in $A(\lambda)$ have occurred over the 24 hour period. In Experiment A, however, changes in cloud base buoyancy oppose changes in buoyancy above cloud base at almost all time steps. In the Amazon Basin, the changes in the individual terms are large, apparently in response to the strong continental diurnal cycle, but the implied change in $A(\lambda)$ is much less. At a Marshall Islands grid point in the West Pacific, variations in the individual buoyancy terms are themselves small as well as being negatively correlated; the fluctuations seem to be due primarily to weak semidiurnal forcing. At both points the atmosphere nearly returns to its initial state after 24 hours. This demonstrates that a simple closure at cloud base combined with penetrative convection physics above cloud base can produce $dA(\lambda)/dt \approx 0$.

The improvements of Experiment A over the control indicate a more realistic response of the atmosphere to convective heating, i.e., the calculated convective mass fluxes better represent the effects of large-scale forcing by low-level convergence and surface fluxes. It is interesting to compare this experiment, in which M_c is computed implicitly, to a previous experiment in which M_c is based explicitly on estimates of the large-scale forcing (Experiment Z of DY88). Table 2 gives selected climate parameters for both experiments as well as the control run (Model II). Despite the completely different approaches for computing M_c, the two experiments give almost identical results in the global and time mean; each, however, differs substantially from the control. Many of the regional changes in convection are also similar in the two experiments (compare, e.g., Figs. 2–4 of this paper with Figs. 3–5 of DY88). This can be interpreted as an indirect GCM verification of the quasi-equilibrium hypothesis.

One difficulty with Experiment A is its vertical profile of cumulus heating in the tropics (Fig. 7). The control run, which overstabilizes the atmosphere after moist

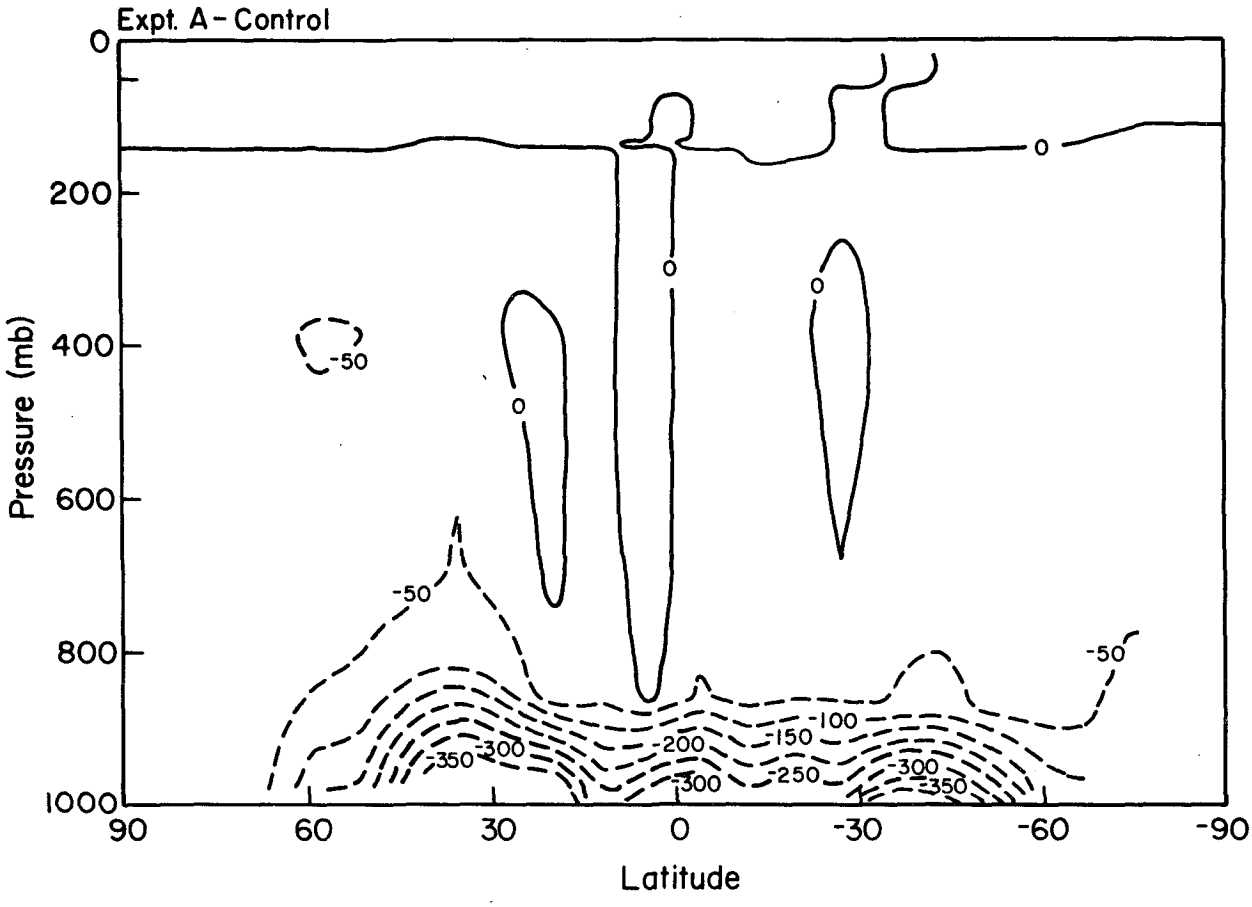

FIG. 4. Differences in zonal mean cumulus mass exchange (10^9 kg s^{-1}) between Expt. A and the control.

convective events, actually produces a realistic bimodal spectrum of convective cloud top heights as a result (see Table 5 and discussion later in this section). Experiment A, which marginally stabilizes the atmosphere, has a tendency to produce mostly deep convective events in the tropics instead. The convective heating is thus concentrated at upper levels (peaking at 320 mb). Diagnosed heating profiles for the most convectively active regions of the tropics show heating peaking at lower levels, $p \geq 400$ mb (Thompson et al. 1979). This discrepancy apparently occurs because the cloud parcels in our experiment rise undiluted by less buoyant environmental air. It is therefore instructive to examine the effect of entrainment.

Experiment B is identical to Experiment A, except that the fractional rate of entrainment is set at $\lambda = 0.2$ km^{-1}, a value intermediate to that characteristic of deep and shallow clouds in the mean (Lord and Arakawa 1980). [According to Simpson et al. (1965), $\lambda = 2\alpha/R$ with R being the cloud radius and α the entrainment constant; then for $\alpha = 0.1$, $\lambda = 0.2$ km^{-1} corresponds to $R = 1$ km.] The entrainment causes plumes to lose buoyancy at a lower level; this shifts the convective heating profile downward by 150 mb (Fig. 7), more consistent with observations. However, rather than producing a cloud-top height spectrum with a single peak in the midtroposphere, the experiment produces a bimodal spectrum of deep and shallow clouds in response to the time-varying vertical structure. The global mean occurrence frequency of deep convection decreases from 23% to 10%. Associated with this, tropical upper troposphere specific humidities are reduced to more realistic values (Table 3), compared with values interpolated from observations compiled by Oort (1983). (This is of little concern for the convection itself but crucial for simulating cirrus cloud cover, cloud-radiation feedback, and upper troposphere chemical reactions.) Unfortunately, Experiment B also undesirably reduces the specific humidities just above the PBL.

Entrainment also affects the distribution of eddy kinetic energy in the tropics because of parameterized momentum mixing ("cumulus friction"). This is an important consideration for our model, whose winds are used as inputs for chemical tracer transport simulations. Results from Model II indicate that it produces insufficient interhemispheric transport (Prather et al. 1987); a deficiency of eddy energy at the equator

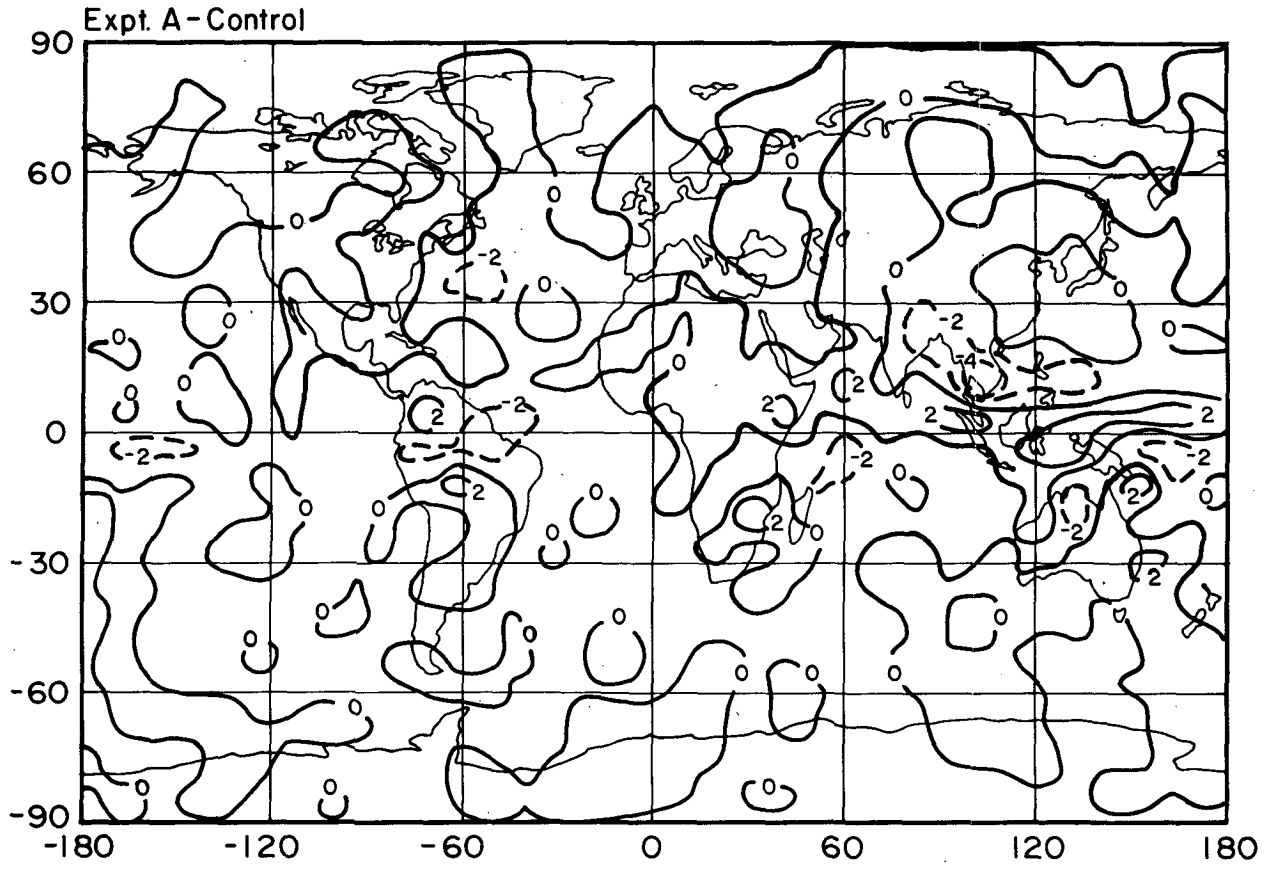

FIG. 5. As in Fig. 2 but for differences in precipitation (mm day^{-1}).

is one possible cause. This deficiency most likely is concentrated in long waves; the GCM without entrainment generates 1.3 times as much equatorial eddy energy in wavenumbers 1–3 as in wavenumbers 4–6 (Table 4). Tropopause data analyzed by Julian et al. (1970) suggest a ratio of 1.8 instead. Experiment B, on the other hand, dissipates less kinetic energy because fewer plumes reach the tropopause, where winds are strongest and cumulus friction greatest. As a result, longwave energy increases dramatically, by a factor of 3.6 (Table 4), far in excess of that observed. A separate experiment with $\lambda = 0.1$ km^{-1} generally produces results intermediate to those of Experiments A and B.

Taken together, these simulations suggest that a moderate amount of entrainment can reduce upper tropospheric cumulus mass fluxes to the extent needed to produce a realistic simulation of tropopause conditions. However, the associated reduction in deep convection occurrence frequency is inconsistent with ISCCP observations (Del Genio and Yao 1987). The implication is that our closure scheme without entrainment produces a realistic number of events but with too much mass reaching the tropopause in each event. An obvious explanation is that the available M_c at cloud base is partitioned among clouds with different λ, those with higher values of λ detraining at low levels and only those with minimum λ reaching the tropopause. This approach to modeling of a cumulus ensemble has been discussed by Arakawa and Schubert (1974) and Yanai et al. (1973). To test the importance of this partitioning, we conducted two experiments (C and D) with two cloud types.

In Experiment C, each plume has a mass of $0.5M_c$, one with no entrainment and the other with $\lambda = 0.2$ km^{-1}. In Experiment D, one plume has $0.25M_c$ with no entrainment, while the other one has $0.75M_c$ with $\lambda = 0.2$ km^{-1}. Physically, these experiments may be viewed as crudely resolving a cloud cluster into a protected undilute "core" and surrounding updrafts in direct contact with the environment. As shown in Table 3, experiment C does not significantly reduce the specific humidities in the upper atmosphere at 4°N, while Experiment D produces a realistic humidity profile throughout the upper atmosphere. Each experiment increases equatorial eddy kinetic energy, D more so than C since a smaller fraction of its M_c is nonentraining (Table 4). Both experiments give a fairly realistic ratio of longwave/synoptic scale eddy energy. Both experiments also produce desirable frequencies of deep convection, as expected, since some of the mass always

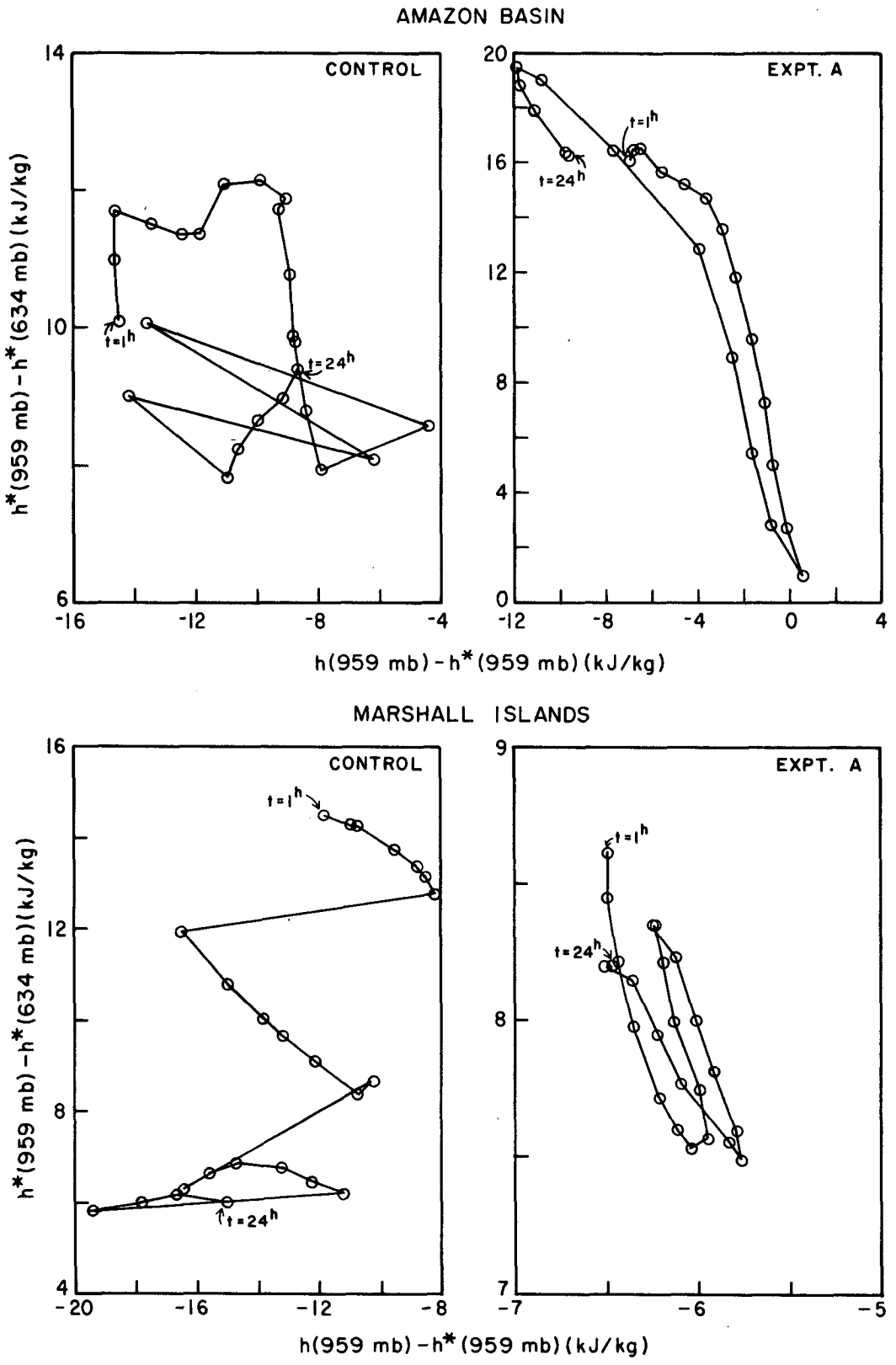

FIG. 6. Hourly evolution of conditional instability between 959 mb (l = 1) and 634 mb (l = 4) vs cloud base buoyancy at 959 mb for the last 24 hours of the control run and Expt. A. Top: Amazon Basin (4°S, 60°W). Bottom: Marshall Islands (4°N, 160°E).

TABLE 2. Comparison of globally averaged convection and cloud parameters produced by the GCM using three different cumulus mass flux closure assumptions: 50% of the cloud-base grid box (Model II), neutral buoyancy at cloud base (Experiment A), and mass flux calculated directly from large-scale forcing terms (Experiment Z of DY88).

	Model II	Neutral buoyancy	Large-scale forcing
Cumulus mass exchange (10^9 kg s^{-1})	1868	1384	1334
Cumulus heating (W m^{-2})	88	80	79
Precipitation (mm day^{-1})	2.93	2.76	2.80
Total cloud cover (%)	45.1	43.3	43.1
High	21.4	22.6	21.8
Middle	15.2	16.1	16.4
Low	34.8	33.4	33.4
Net downward radiation at top of atmosphere (W m^{-2})	15.2	18.3	18.2
Net downward energy flux at surface (W m^{-2})	24.6	26.8	26.6

penetrates without dilution (25.8% for both experiments in the global average). The cumulus heating profile, not surprisingly, is a hybrid of those for Experiments A and B (Fig. 7). Experiment D further shifts the peak precipitation from its 4°N location in Experiments A, B and C to 4°S, in good agreement with available January observations (Jaeger 1976).

One undesirable feature of all the experiments is that specific humidities in the lower atmosphere at 4°N are lower than observations (Oort 1983). The moisture budget of this part of the atmosphere is strongly influenced by shallow convection. The dryness of our lower troposphere does not seem to be due to insufficient shallow convection, because the humidity there actually decreases with increasing shallow convection proceeding from Experiment A to C to D. A separate experiment in which the efficiency of condensate reevaporation is increased for shallow clouds affects the subtropics but has little impact at the equator. The saturated convective-scale downdrafts proposed by DY88 seem to be the most likely way to remedy this deficiency. Another possibility is that reevaporation of condensate from deep clouds is underestimated in the absence of an accurate microphysical parameterization.

Since entrainment rates cannot be predicted from first principles given current understanding of the process, a practical strategy for prescribing them in a GCM might involve comparison of the simulated cumulus spectrum with observations. To facilitate this, we have analyzed the convective frequencies from the last day of integration of Experiment D. Out of 2120 convection occurrences in which the nonentraining plume penetrated from level 1 to level 7, the frequency of occurrence for the second plume's top at levels 2 through 6 are 19.3, 30.4, 13.2, 11.5 and 25.6%, respectively. In other words, in deep convection situations the model sometimes generates 2 deep plumes (as might be the case, e.g., in the trough of an easterly wave), while at other times it predicts simultaneous deep and shallow events. The time-averaged mass flux spectrum, though, is clearly bimodal, as discussed subsequently (see also Fig. 7). Similar results also appear in Experiment C. Thus, despite the crude representation of the cumulus cloud spectrum, Experiments C and D produce a convective mass distribution similar to observations (Johnson 1976; Nitta 1978). The shape of the spectrum in our experiments depends on the assumed value of λ, but its bimodal character is a direct consequence of the large-scale thermodynamic structure, since the closure we use places no explicit constraint on the levels above cloud base. This differs somewhat from the Arakawa–Schubert scheme, in which the spectrum depends on the vertical structure indirectly through the requirement for quasi-equilibrium. For the λ chosen here, more convection penetrates to level 3 than to level 2; this can be altered by increasing λ to match estimates better for shallow clouds. Bimodality is not characteristic of all convective situations, however. For example, when the cloud base is higher or the cloud top of the first plume is lower, a unimodal distribution is often obtained. These occur infrequently, though, so that our estimates for a 24-hour period may not be statistically significant.

Several datasets for deep and shallow convection are available as benchmarks for experiments. Diagnoses of the cumulus mass flux spectrum in areas of intense

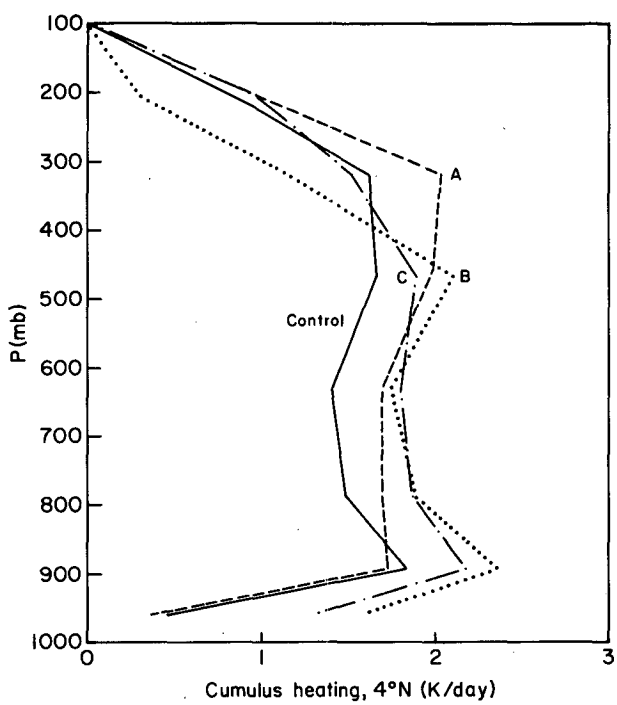

FIG. 7. Vertical profiles of zonal mean cumulus heating rate (K/day) in the tropics for the control and Expts. A, B and C.

TABLE 3. Zonal mean specific humidity (g kg^{-1}) profiles at 4°N for each of the experiments vs. observations.

Level	Pressure (mb)	Oort (1983)	Control	Expt. A	Expt. B	Expt. C	Expt. D
7	201	<0.05	0.10	0.10	0.04	0.09	0.06
6	321	0.33	0.7	0.7	0.4	0.5	0.4
5	468	1.5	2.1	2.3	1.2	1.8	1.4
4	634	4.1	4.5	4.8	3.1	3.5	2.9
3	786	8.0	7.3	7.4	6.1	6.2	5.7
2	894	11.8	10.5	10.3	10.0	9.7	9.4
1	959	14.7	14.2	14.6	15.2	14.9	14.5

deep convection, for example, usually show comparable amounts of deep and shallow convection when downdraft effects are included (Johnson 1976; Nitta 1978). In suppressed trade cumulus regions, however, the shallow cumulus mass flux is an order of magnitude greater (Nitta 1975). ISCCP data for the tropical Pacific when El Niño is not occurring suggest that deep convection in the West Pacific is ≈2.5–5.5 times more frequent than in the East Pacific (Fu 1988). Table 5 shows the GCM-simulated ratios of deep to shallow convective frequency for the West Pacific and Hawaii, and for each convection type, the ratio of its occurrence in the West Pacific to that in the East Pacific. The deep/shallow frequency ratios in this table are multiplied by an analogous ratio of convective mass exchange per event to indicate the relative amounts of deep and shallow cumulus mass flux produced by the simulations. Without entrainment, a realistic closure for cloud base mass flux clearly produces excessive deep convection. Entrainment acting on a single plume produces roughly equal amounts of deep and shallow convection in the West Pacific as observed, but suppresses deep convection in the more stable East Pacific to a greater extent than ISCCP data suggest. With two plumes, though, both the spectrum of convective cloud top height and its geographic variation can be simulated realistically; this is especially true of Experiment D.

6. Summary and conclusions

An improved version of the GISS Model II cumulus parameterization, designed specifically for use in long-term climate studies, has been used to examine the effects of entrainment and multiple cloud types on a January climate simulation. Instead of prescribing convective plume mass as a fixed fraction of the cloud base grid box mass, we calculate the convective mass based on the closure assumption that the cumulus convection restores the atmosphere to a neutral moist convective state. This change alone significantly improves several aspects of the January climate: the precipitation distribution, cumulus mass exchanges, and deep convection occurrence frequencies. Variations in vertical structure in the tropics are consistent with the quasi-equilibrium hypothesis.

Without analytical means for determining the fractional rate of entrainment, λ, we simply prescribe the value of λ within the observational range in experiments intended to evaluate its effect on the climate simulation. The results show that entrainment limits the penetration depth of deep convection, lowers the altitude of peak convective heating, reduces specific humidities in the upper atmosphere to more realistic values, and increases the eddy kinetic energy at the equator, especially at low wavenumbers. For climate change experiments one would ideally prefer to predict λ rather than specify it. However, experiments we conducted with values of λ higher or lower by a factor of 2 did not differ substantially from those discussed here. This suggests that the answers to first-order questions about climate change may not be overly sensitive to the precise value of entrainment rate.

In similar fashion, we investigate the effect of representing convection as a single plume as opposed to a cumulus spectrum by simply dividing the plume mass

TABLE 4. Simulated equatorial tropospheric eddy kinetic energy (10^4 J m^{-2}) and its ratio between different longitudinal wavenumber (n) ranges.

	Energy (n = 1–3)	Ratio [(n = 1–3)/(n = 4–6)]
Control	7.42	1.32
A	6.47	1.35
B	23.15	2.06
C	8.66	1.52
D	10.91	1.58

TABLE 5. Convective occurrence frequency ratios for each of the experiments vs. observations (cited in text). The deep/shallow ratios are multiplied by the ratio of deep/shallow mean mass flux per event for comparison with the observed mass flux spectrum.

	Deep/Shallow		W. Pacific/E. Pacific	
Experiment	W. Pacific	Hawaii	Deep	Shallow
Control	0.6	0.1	2.0	0.6
A	∞	0.3	5.1	0.0
B	1.3	0.3	13.3	0.7
C	3.5	0.1	3.7	0.4
D	1.1	0.2	3.4	0.8
Observations	≈1	≤0.1	≈2.5–5.5	?

into two specified parts, one with no entrainment and the other with a prescribed λ. Despite the simplicity of this approach, we produce a clear bimodal distribution of convective mass flux (in regions of strong convection) whose vertical and geographic distributions are consistent with field studies and ISCCP data for the tropics. This crude approximation to a cumulus spectrum retains many desirable features of the simulated January climate. Since using a single cloud type without entrainment is as arbitrary as using multiple cloud types with prescribed fractional rates of entrainment, it is desirable to use the latter approach because it produces a significantly better climate simulation. [One possibility for determining rather than prescribing M_1 is to calculate the convective mass flux based only on low-level convergence as given by Eq. (1) in DY88; then $M_2 = M_c - M_1$. As shown in DY88, M_1 calculated this way produces mostly deep convection. We have conducted an experiment which partitions M_1 and M_2 in this fashion; it produces results similar to those of Experiments C and D.] We conclude that the cumulus parameterization proposed here is a workable scheme for use in current climate simulations and climate sensitivity studies, especially in combination with a downdraft parameterization such as that proposed by DY88.

One shortcoming of the present model is its use of temperature rather than virtual temperature as the basis for calculating the buoyancy of cloud parcels. The contribution from varying water vapor concentration can be included in straightforward fashion; its effect is to increase the degree of instability slightly and, therefore, to increase the cumulus flux required for neutral buoyancy. The negative buoyancy effect of condensate loading is more difficult to estimate because it depends on details of the microphysics of the cloud. Betts (1982) has shown that in the limit of pure adiabatic uplift (no precipitation or dilution by entrainment), parcels rise with nearly neutral buoyancy in typical tropical environments. However, adiabatic liquid water contents are rarely observed in actual convective clouds (Ackerman 1963; Warner 1970), so the idealized situation studied by Betts should be regarded as defining only a lower limit for the buoyancy. Nonetheless, some reduction in buoyancy due to condensate loading should be incorporated in future versions of all penetrative cumulus parameterizations.

DY88 calculated convective mass fluxes by use of a relationship between the cumulus mass flux, low-level convergence, surface evaporation, and the time rate of change of boundary layer height [Eq. (4) in DY88]. It is interesting to note that many of the improvements in the January climate obtained here were also achieved by the completely different closure assumption of DY88. In particular, both schemes give similar global mean cumulus mass fluxes and convective heating. However, if we calculate M_c using the closure assumption suggested here, the equation used by DY88 to predict M_c can be readily used instead for predicting boundary layer heights as in Randall et al. (1985). On the other hand, the scheme proposed here may be regarded as setting an upper limit on the cumulus mass flux, with the parameterization of DY88 providing a lower value for use in unstable but suppressed convective environments. Given the similarity of the global simulations produced by these schemes, the differences between the two are likely to be restricted to details of the regional response to climate forcing or the depiction of transient events.

Acknowledgments. We wish to thank J. Hansen, S. Lord, P. Stone, and R. Suozzo for many useful comments. We are also indebted to G. Russell, R. Ruedy, R. Suozzo, and J. Lerner for their help with GCM diagnostic and physics routines. The figures were drafted by J. Mendoza and L. del Valle. This research was supported by the NASA Climate Program.

REFERENCES

Ackerman, B., 1963: Some observations of water contents in hurricanes. *J. Atmos. Sci.*, **20**, 288–298.

Albrecht, B. A., 1983: A cumulus parameterization for climate studies of the tropical atmosphere. Part I: Model formulation and sensitivity tests. *J. Atmos. Sci.*, **40**, 2166–2182.

Arakawa, A., 1972: Parameterization of cumulus convection: Design of the UCLA general circulation model. Numerical Simulation of Weather and Climate, Tech. Rep. No. 7, Dept. of Meteorology, University of California, Los Angeles.

——, and W. H. Schubert, 1974: Interaction of a cumulus cloud ensemble with the large-scale environment. Part I. *J. Atmos. Sci.*, **31**, 674–701.

——, and J.-M. Chen, 1987: Closure assumptions in the cumulus parameterization problem. *Short- and Medium-Range Numerical Weather Prediction*, Suppl. to *J. Meteor. Soc. Japan*, 107–131.

Baker, W. E., E. C. Kung and R. C. J. Somerville, 1977: Energetics diagnosis of the NCAR general circulation model. *Mon. Wea. Rev.*, **105**, 1384–1401.

Betts, A. K., 1982: Saturation point analysis of moist convective overturning. *J. Atmos. Sci.*, **39**, 1484–1505.

——, 1986: A new convective adjustment scheme. Part I: Observational and theoretical basis. *Quart. J. Roy. Meteor. Soc.*, **112**, 677–691.

Del Genio, A. D., and M.-S. Yao, 1987: Properties of deep convective clouds in the ISCCP Pilot Data Set. Preprints, *17th Conf. on Hurricanes and Tropical Meteorology*, Miami, Amer. Meteor. Soc., 133–136.

——, and ——, 1988: Sensitivity of a global climate model to the specification of convective updraft and downdraft mass fluxes. *J. Atmos. Sci.*, **45**, 2641–2668.

Fu, R., 1988: Properties of deep convective clouds in the tropical Pacific from analysis of ISCCP radiances. M.S. thesis, Dept. of Geological Sciences, Columbia University, 52 pp.

Gerald, C. F., 1980: *Applied Numerical Analysis.* Addison-Wesley, 518 pp.

Hansen, J., G. Russell, D. Rind, P. Stone, A. Lacis, S. Lebedeff, R. Ruedy and L. Travis, 1983: Efficient three-dimensional global models for climate studies: Models I and II. *Mon. Wea. Rev.*, **111**, 609–662.

——, A. Lacis, D. Rind, G. Russell, P. Stone, I. Fung, R. Ruedy and J. Lerner, 1984: Climate sensitivity: Analysis of feedback mechanisms. *Climate Processes and Climate Sensitivity*, J. E. Hansen and T. Takahashi, Eds., Amer. Geophys. Union, 130–163.

Jaeger, L., 1976: Monatskarten des hiederschlags fürdie ganze erde. *Ber. Dtsch. Wetter dienstes, No. 139*, Band 18. Offenbach A.M., 38 pp and plates.

Johnson, R. H., 1976: The role of convective-scale precipitation downdrafts in cumulus and synoptic-scale interactions. *J. Atmos. Sci.*, **33**, 1890–1910.

——, 1980: Diagnosis of convective and mesoscale motions during Phase III of GATE. *J. Atmos. Sci.*, **37**, 733–753.

Julian, P. R., W. M. Washington, L. Hembree and C. Ridley, 1970: On the spectral distribution of large-scale atmospheric kinetic energy. *J. Atmos. Sci.*, **27**, 376–387.

Knupp, K. R., and W. R. Cotton, 1985: Convective cloud downdraft structure: An interpretive survey. *Rev. Geophys.*, **23**, 185–215.

Kuo, H. L., 1965: On formation and intensification of tropical cyclones through latent heat release by cumulus convection. *J. Atmos. Sci.*, **22**, 40–63.

——, 1974: Further studies of the parameterization of the influence of cumulus convection on large-scale flow. *J. Atmos. Sci.*, **31**, 1232–1240.

Lindzen, R. S., A. Y. Hou and B. F. Farrell, 1982: The role of convective model choice in calculating the climate impact of doubling CO_2. *J. Atmos. Sci.*, **39**, 1189–1205.

Lord, S. J., 1982: Interaction of a cumulus cloud ensemble with the large-scale environment. Part III: Semi-prognostic test of the Arakawa-Schubert cumulus parameterization. *J. Atmos. Sci.*, **39**, 88–103.

——, and A. Arakawa, 1980: Interaction of a cumulus cloud ensemble with the large-scale environment. Part II. *J. Atmos. Sci.*, **37**, 2677–2692.

——, W. C. Chao and A. Arakawa, 1982: Interaction of a cumulus cloud ensemble with the large-scale environment. Part IV: The discrete model. *J. Atmos. Sci.*, **39**, 104–113.

Manabe, S., J. Smagorinsky and R. F. Strickler, 1965: Simulated climatology of a general circulation model with a hydrological cycle. *Mon. Wea. Rev.*, **93**, 769–798.

Nitta, T., 1975: Observational determination of cloud mass flux distributions. *J. Atmos. Sci.*, **32**, 73–91.

——, 1978: A diagnostic study of interaction of cumulus updrafts and downdrafts with large-scale motions in GATE. *J. Meteor. Soc. Japan*, **56**, 232–241.

Oort, A. H., 1983: Global atmospheric circulation statistics, 1958–1973. NOAA Prof. Pap. 14, U.S. Dept. of Commerce, Washington, DC, 180 pp.

Paluch, I. R., 1979: The entrainment mechanism in Colorado cumuli. *J. Atmos. Sci.*, **36**, 2467–2478.

Prather, M., M. McElroy, S. Wofsy, G. Russell and D. Rind, 1987: Chemistry of the global troposphere: Fluorocarbons as tracers of air motion. *J. Geophys. Res.*, **92**, 6579–6613.

Randall, D. A., J. A. Abeles and T. G. Corsetti, 1985: Seasonal simulations of the planetary boundary layer and boundary-layer stratocumulus clouds with a general circulation model. *J. Atmos. Sci.*, **42**, 641–676.

Riehl, H., and J. S. Malkus, 1958: On the heat balance in the equatorial trough zone. *Geophysica*, **6**, 503–538.

Simpson, J., R. H. Simpson, D. A. Andrews and M. A. Eaton, 1965: Experimental cumulus dynamics. *Rev. Geophys.*, **3**, 387–431.

Sloss, P. W., 1967: An empirical examination of cumulus entrainment. *J. Appl. Meteor.*, **6**, 878–881.

Thompson, R. M., Jr., S. W. Payne, E. E. Recker and R. J. Reed, 1979: Structure and properties of synoptic-scale wave disturbances in the intertropical convergence zone of the eastern Atlantic. *J. Atmos. Sci.*, **36**, 53–72.

Warner, J., 1970: On steady-state one-dimensional models of cumulus convection. *J. Atmos. Sci.*, **27**, 1035–1040.

Wetherald, R. T., and S. Manabe, 1988: Cloud feedback processes in a general circulation model. *J. Atmos. Sci.*, **45**, 1397–1415.

Yanai, M., 1971: A review of recent studies of tropical meteorology relevant to the planning of GATE. *Experiment Design Proposal for the GARP Atlantic Tropical Experiment*, Vol. 2, Annex I, ICSU/WMO, 188 pp.

——, S. Esbensen and J.-H. Chu, 1973: Determination of bulk properties of tropical cloud clusters from large-scale heat and moisture budgets. *J. Atmos. Sci.*, **30**, 611–627.

Yao, M.-S., and P. H. Stone, 1987: Development of a two-dimensional zonally averaged statistical-dynamical model. Part I: The parameterization of moist convection and its role in the general circulation. *J. Atmos. Sci.*, **44**, 65–82.